Korean Journal of Chemical Engineering (2024) 41:2461–2476
https://doi.org/10.1007/s11814-024-00199-x

REVIEW ARTICLE

Metal–Organic Frameworks for Aromatic-Based VOC Decomposition

Thach N. Tu[1,2] · Nhung Thi Tran[3] · Quoc Hao Nguyen[1] · Van Nhieu Le[4] · Jinsoo Kim[1]

Received: 11 April 2024 / Revised: 14 May 2024 / Accepted: 27 May 2024 / Published online: 8 June 2024

Abstract
Metal–organic frameworks (MOFs) are a class of porous materials based on the strong coordinated bonds between inorganic secondary building units (SBUs) and organic linkers to form high-porosity periodic structures. MOFs with tunable pore size, shape, and catalysis active sites recently sparked recognition interest for the design and synthesis of catalysts with the capability to decompose aromatic-based VOCs. In this review, we introduce our viewpoints for the design and synthesis of better MOF-based photocatalysts including (i) methods to enhance the interaction of aromatic-based VOCs with MOFs by controlling micropore size, tuning Lewis acidity of the metal SBUs and/or using linkers bearing electron withdrawal groups; (ii) methods to enhance adsorption/diffusion by synthesizing hierarchical MOFs through defect control, reticular structural design and/or employing the xerogel monoliths to exploit the mesopore between particles for enhancing the adsorption/diffusion; (iii) methods to optimize the band gap by selecting appropriate building block and/or doping with exotic components. Alongside that, design principles and strategies for the development of MOF-based catalysts for thermal decomposition of aromatic-based VOCs are also provided such as (i) the need to improve the thermal stability at high temperature together with a slit pore architecture connected by small windows to prevent the aggregation of active components; and (ii) methods to control the distribution and type of active components in the MOFs' matrix to alter their catalysis performance. We expect our discussion and viewpoints on the design and synthesis of MOFs and MOF-based composites to inspire researchers to design better and more efficient systems for aromatic-based VOC decomposition.

Keywords Metal–organic frameworks (MOFs) · Reticular chemistry · Porous materials · Volatile organic compounds · VOCs decomposition · Photocatalysis · Thermal decomposition

Introduction

Aromatic-based volatile organic compounds (VOCs), such as benzene, toluene, xylene, ethylbenzene, styrene, etc., can cause severe harm to human health [1]. Benzene, a common chemical substance emitted from burning coal and oil, gasoline service station, and motor vehicle exhaust, is classified as a Group 1 human carcinogen [2]. The high toxicity of benzene led to an effort to avoid its use in industrial production. On the other hand, alternative substances used in industrial production, such as toluene, ethylbenzene, and xylenes (TEX), also cause severe harm to human health upon long-term exposure [3, 4]. Commonly, these TEX compounds are found in the emission of industrial production and fossil fuel-powered vehicles as well as in indoor air at a relatively low concentration. The low concentration of TEX, coupled with their susceptibility to oxidation decomposition under mild conditions, makes it more convenient and economical to develop catalysts for directly decomposing or mineralizing them into H_2O and CO_2.

Metal–organic frameworks (MOFs) is a class of porous materials based on the strong coordinated bonds between inorganic secondary building units (SBUs) and organic linkers to form high-porosity periodic structures [5, 6]. The assembled

✉ Jinsoo Kim
jkim21@khu.ac.kr

1 Department of Chemical Engineering (Integrated Engineering), Kyung Hee University, 1732 Deogyeong-daero, Giheung-gu, Yongin-si, Gyeonggi-do 17104, Republic of Korea

2 Nguyen Tat Thanh University, 300A Nguyen Tat Thanh Street, District 4, Ho Chi Minh City 755414, Vietnam

3 Ho Chi Minh City University of Technology and Education (HCMUTE), 01 Vo Van Ngan Street, Thu Duc District, Ho Chi Minh City 720100, Vietnam

4 Faculty of Chemical Engineering, Industrial University of Ho Chi Minh City, 12 Nguyen Van Bao Go Vap, Ho Chi Minh City 70000, Vietnam

principle relies on the defined SBUs and organic linkers leading to the possibility for the design and synthesis of MOFs [7]. Alongside these, the selection of organic linkers bearing a desired functionality and/or SBUs allows MOFs to be designed with tunable pore size and chemical properties for a myriad of practical applications. These include catalysis [8–13], gas/vapor storage [14–17], capture [18–20] and separations [21–27], proton conduction [28–31], and controlled delivery of guest molecules [32–36]. In these applications, the flexibility in structural design and synthesis has sparked significant interest in the utilization of MOFs for capturing aromatic-based VOCs [19, 37] and/or facilitating their decomposition [38, 39]. For example, the incorporation of metal clusters, metal complexes, nanoparticles, and/or active organic centers enables the use of MOFs as effective catalysts for the decomposition of aromatic-based VOCs [38, 39]. However, the typically low VOC concentration in air can render MOF-based catalysts ineffective for VOC decomposition, because they fail to concentrate the VOCs around the active centers. This has raised the demand for the design and synthesis of MOF-based catalysts with the capacity to capture and decompose TEX at low concentrations.

Recently, the growing interest in this field has sparked demands to summarize progress in the design and synthesis of MOF-based catalysts for TEX decomposition [40]. For example, the design and synthesis of Zr-MOFs and MIL-125(Ti)-based catalysts for the removal of environmental pollutants, such as VOCs, CO_x and CH_4, heavy metals, organic antibiotics, and dyes, have gained tremendous interest from the research community [41, 42]. In the other case, the effect of different parameters, such as catalyst surface metal capacity and oxygen species in the oxidation of toluene and other VOCs, together with the plausible mechanisms are discussed [43]. Alongside, there are other reviews for VOC degradation technologies using MOF-derived materials and different types of materials [44, 45]. These reviews, however, are limited to particular MOF-based materials, and/or metal oxides for general VOC decomposition. In this sense, this review summarizes the recent advances alongside our viewpoints for the design and synthesis of MOF-based catalysts for aromatic-based VOC decomposition with an enhancing catalytic activity. We expect this review to provide the basis for assisting further material design to develop MOFs as effective catalysts for aromatic-based VOC decomposition.

MOFs for Photocatalytic Decomposition of Aromatic-Based VOCs

Despite the fast growth, current research to develop MOF-based catalysts for aromatic-based VOC decomposition showed drawbacks related to the need for catalyst improvement. Recent studies employed a large quantities of adsorbents and/or catalysts for the aromatic-based VOC mineralization due to the need to capture and concentrate the VOCs from the surrounding environment and/or the low catalytic activity of the active centers. In terms of engineering design, the lack of a method for fabricating the transparent catalyst frame/film, together with the shortage of investigations on stacking these catalyst layers, makes the practical use of this technique a long process. The summary of the recent advances in catalysis design and the fabrication of the supporting catalyst frame for VOC decomposition is presented below.

Photocatalytic mineralization has some major advantages for wide applications in treating indoor VOCs due to the mild working conditions and energy saving using sunlight as illumination source. In the photocatalysis system, MOFs often play a major role in concentrating VOCs around catalytic active centers (i.e., metal clusters and nanoparticles) by adsorbing them from the ambient atmosphere at very low concentrations. This requires MOFs to have a strong interaction and a high uptake of VOCs at the low-pressure region, highlighting the quest to address the fundamental question of how to improve the uptake capacity of VOCs at low concentrations.

Despite these advantages, the reliance on sunlight illumination for operation is a drawback as sunlight may not always be available. This triggered the quest to enhance the quantum efficiency of catalysis to reduce the time required for VOC decomposition/mineralization. For convenience and energy-saving purposes, photocatalysts should be capable of adsorbing and storing VOCs without releasing them when sunlight is unavailable. To minimize leakage, ideal MOFs must exhibit minimal changes in uptake capacity due to fluctuations in ambient temperature [19, 37].

Catalysis System Based on Iron-MOFs

Several MOFs play multiple roles in the photocatalyst system. MOFs serve as adsorbents for VOC concentration and as active catalysts, with metal clusters acting as the active sites and linkers functioning as antennas that absorb photons from incident light. Several studies have revealed the excellent performance of iron-based MOFs in the photocatalytic decomposition of toluene and xylene due to their ability to interact with O_2 and generate active $O_2^{\bullet-}$. Zhang et al. employed NH_2-MIL-101(Fe) hexagonal microspindles (MIL = Matériaux de l′Institut Lavoisier) for the photocatalytic degradation of toluene under visible-light illumination [46]. This photocatalyst demonstrated enhanced performance for toluene degradation under visible light compared to nano-$BiVO_4$/TiO_2 and quantum-$BiVO_4$, achieving 79.4% toluene conversion. The catalysis mechanism of NH_2-MIL-101(Fe) was investigated using the in-situ

Fourier-transform infrared spectroscopy (FT-IR) technique, revealing that both amine functionality and Fe clusters were excited under visible-light illumination to generate photo-induced electrons and holes. Subsequently, the photogenerated electrons from the amine were then transferred to the Fe clusters via the ligand-to-cluster charge-transfer mechanism. The Fe clusters were excited like the semiconductor and served as active sites to react with O_2, generating active $O_2^{\cdot-}$, which subsequently participated in the reaction with adsorbed toluene molecules (Table 1, Entry 1) [46].

Li et al. also utilized the MIL-88(B) photocatalyst in a process involving two consecutive steps: toluene adsorption/removal and the subsequent photocatalytic decomposition of the adsorbed molecules under simulated sunlight irradiation (Fig. 1) [47]. Under optimized conditions, MIL-88(B) achieved 100% adsorption/removal efficiency of toluene at an initial concentration of 460 ppm. The adsorbed toluene was then successfully decomposed to CO_2 with 85% selectivity under 1 SUN irradiation. In the overall performance, the entire cycle took approximately 100 min for full catalyst regeneration. The mechanism studies revealed the principal role of the ·OH and h^+ generated at the photo-excited Fe cluster for toluene mineralization (Fig. 1, Table 1, Entry 2) [47]. Despite initial success, MIL-88(B) exhibited low catalysis performance. Indeed, a significantly large amount of MIL-88(B) was required compared to NH_2-MIL-101(Fe) to achieve a similar reaction rate. This can be attributed to the low surface area of the guest-free MIL-88(B), which hinders the adsorption and oxidation of toluene.

Further extending the pore size of Fe-based MOF using MIL-100 resulted in reduced performance. The fabrication of a photocatalytic metal–organic framework filter (PMF) through the electrophoretic deposition of MIL-100(Fe) nanoparticles on porous nickel foam and its performance on adsorption and decomposition of BTEX under UV light was examined [48]. The system exhibited a VOC conversion of 75.95% after 30 min of irradiation with 0.52 µL of BTEX at a concentration of 10 ppm (Table 1, Entry 3) [48]. The reduced catalytic activity of the system can be attributed to the structural architecture of MIL-100, which consists of very large-pore sizes of 2.5 and 2.9 nm connected by window sizes of 0.55 and 0.88 nm. This structure makes it difficult to adsorb BTEX, resulting in low conversion even under UV light.

The presence of the exotic component in MIL-100 may result in synergistic effects via a heterojunction mechanism, leading to improve the catalysis activity. Chen et al. found that composites made from α-Fe_2O_3 and MIL-100 exhibited enhanced performance in the adsorption and photocatalytic oxidation of o-xylene under visible-light irradiation (Fig. 2) [49]. The MIL-100(Fe)/α-Fe_2O_3 hybrid specifically exhibited high efficiency, achieving approximately 100% degradation efficiency of o-xylene under xenon lamp irradiation and 90% under visible light ($\lambda \geq 420$ nm) for more than 300 min of exposure under a continuous flow rate of 10 mL/min and a concentration of 50 ppm. This value was superior to that of MIL-100(Fe) (80% under 250 W Xe lamp irradiation and 75% under visible light) or TiO_2 (23% under 250 W Xe lamp irradiation and 0% under visible light). The 5,5-dimethyl-1-pyrroline N-oxide (DMPO) spin-trapping electron paramagnetic resonance (ESR) spectra showed the participations of both ·OH and $O_2^{\cdot-}$ for MIL-100(Fe)/α-Fe_2O_3, while only ·OH or $O^{\cdot 2-}$ was found for α-Fe_2O_3 or MIL-100(Fe), respectively. The observed band-gap energy for α-Fe_2O_3 and MIL-100(Fe), together with the oxidation potential of H_2O/·OH and the reduction potential of O_2 to $O_2^{\cdot-}$, led the authors to depict a photocatalysis mechanism in which both α-Fe_2O_3 and MIL-100(Fe) are excited under visible-light illumination. The electrons generated at the conduction band (CB) of α-Fe_2O_3 then transfer to the valence band of MIL-100(Fe) through the contact interface between α-Fe_2O_3 and MIL-100(Fe) to recombine with the holes (h^+). The electrons generated at the conduction band (CB) of MIL-100(Fe) become more active in reducing O_2 to $O_2^{\cdot-}$. At the same time, the holes generated in the valence band (VB) of α-Fe_2O_3 oxidize H_2O to generate ·OH (Fig. 2, Table 1, Entry 4) [49]. This system appears to work well with o-xylene; however, it is limited for the decomposition of toluene due to the non-suitable band gap.

The above studies indicated the promise of iron-based MOFs for aromatic-based VOCs' decomposition; however, the results still have limitations that require further improvement of catalysts. For example, the iron clusters themselves are active for BTEX oxidation under UV irradiation, while the photocatalysis under visible-light (VIS) illumination showed relatively low activity. Furthermore, the presence of antenna moieties such as amine-based linkers may be needed to improve the catalysis performance. This makes it highly demanded to optimize the band gap of the resulting material by doping suitable antenna moieties to further improve the catalytic activity under VIS irradiation. The optimization of iron-based MOFs, therefore, may focus on several aspects including (i) optimization of adsorption using rigid frameworks with small and large-pore systems (hierarchical MOFs) to enhance both interaction and diffusion; (ii) optimization of the intrinsic catalytic properties of iron-based MOFs by utilizing iron-MOFs built from different metal clusters; (iii) optimization of the band gap by employing iron-based MOFs with photo-antenna moieties on their backbone, such as those synthesized from pyrene and/or porphyrin-based linker, and/or employing exotic components, such as nanoparticles, organic photo-sensitizers, and/or two-dimensional (2D) materials.

Table 1 MOFs for photocatalysis aromatic-based VOC decomposition

Entry	MOF-based catalysts	VOCs	Catalysis condition	Result	References
1	NH_2-MIL-101(Fe)	Toluene	Two consecutive steps of adsorption and catalysis decomposition Visible-light (500 W Xenon lamp), 4 µL toluene, 20 mg catalyst, 6 h irradiation	Conversion of 79.4% Benzoic acid and CO_2 were detected	[46]
2	MIL-88(B)	Toluene	Two consecutive steps of adsorption and catalysis decomposition Solar simulator (100 mW cm^{-2}), 2 µL toluene, 0.2 g catalyst, 50 min irradiation	100% adsorption removal Conversion of 80% after 100 cycles Selectivity of 85% to CO_2	[47]
3	MIL-100(Fe)@ nickel foam	Mixture of benzene, toluene, ethylbenzene, and xylenes (BTEX)	Two consecutive steps of adsorption and catalysis decomposition UV light, ~ 0.52 µL BTEX, conc. of 10 ppm, 30 min irradiation	94.25% adsorption removal BTEX conversion of 75.95% CO_2 was detected	[48]
4	MIL-100(Fe)/α-Fe_2O_3 hybrid	O-xylene	Dynamic adsorption and decomposition with a flow rate of 10 mL/min and conc. of 50 ppm Xenon lamp (250 W) and visible-light irradiation, 95 mg catalyst	100% degradation efficiency of o-xylene under a Xenon lamp (250 W) and 90% under visible light ($\lambda \geq 420$ nm) Working time > 300 min CO_2 was detected	[49]
5	MIL-125(Ti) with the defective site	Toluene	Two consecutive steps of adsorption and catalysis decomposition Solar simulator (100 mW cm^{-2}), 1.0 µL toluene, 0.2 g catalyst, 390 min irradiation	78% mineralization to CO_2	[50]
6	P-MIL-NH_2-125	Toluene	Two consecutive steps of adsorption and catalysis decomposition Visible light (300 W Xe lamp with 420 nm cut-off filter), 1 ml Toluene, 10 mg catalyst, 60 min irradiation	Conversion of 56% 80% mineralization to CO_2	[51]
		Chlorobenzene	Two consecutive steps of adsorption and catalysis decomposition Visible light (300 W Xe lamp with 420 nm cut-off filter), 1 ml Chlorobenzene, 10 mg catalyst, 60 min irradiation	Conversion of 62% 87% mineralization to CO_2	
7	GO/MIL-125(H) hybrid	Toluene	Two consecutive steps of adsorption and catalysis decomposition Solar simulator (100 mW cm^{-2}), 1.0 µL toluene, 0.1 g catalyst, 360 min irradiation	79.22% mineralization to CO_2	[52]
8	UiO-66	Toluene	Dynamic adsorption and decomposition with a flow rate of 20 mL/min and conc. of 20 ppm and air at 10 mL/min Visible light 250 W ($\lambda > 400$ nm), 30 mg catalyst	Capture of 69.6% Photocatalysis decomposition efficiency of 91.2%	[53]

Table 1 (continued)

Entry	MOF-based catalysts	VOCs	Catalysis condition	Result	References
9	TiO_2@NH_2-UiO-66	Styrene	Dynamic adsorption and decomposition with a flow rate of 35 mL/min and conc. of 30 ppm Visible light (300 W xenon lamp with UV filter), 0.1 g catalyst	> 99% mineralization to CO_2 Working time > 600 min	[54]
10	TiO_2-UiO-66-NH_2	Toluene	Dynamic adsorption and decomposition with a flow rate of 100 mL/min and conc. of 25 ppm UV light irradiation, 0.1 g catalyst	Conversion of 72.7% Working time > 720 min CO_2 was detected	[55]
11	TiO_2@UiO-66	Toluene	Dynamic adsorption and decomposition under continuing flow at conc. of 25 ppm UV light, 0.1 g catalyst	Conversion of 66.59% Working time > 720 min	[56]
12	CQDs/UiO-66 MOG	Toluene	Dynamic adsorption and decomposition under continuing flow at conc. 10 ppm of Visible light (250 W xenon lamp with UV filter), 0.5 mg catalyst	Conversion of 35% 85% mineralization to CO_2	[57]
		o-xylene		Conversion of 44% 86% mineralization to CO_2	
		Styrene		Conversion of 29% 30% mineralization to CO_2	
13	Black phosphorus/UiO-66 hybrid	Toluene	Two consecutive steps of adsorption and catalysis decomposition Visible light (300 W Xe lamp), 1.0 µL toluene, 25 mg catalyst, 480 min irradiation Reaction cell of 150 mL and conc. of 2000 ppm	The degradation efficiency of 89.7% with reaction rate of 0.2840 h^{-1} CO_2 was detected	[58]
14	TiO_2@MIL-101	Toluene	Two consecutive steps of adsorption and catalysis decomposition Visible light (300 W Xe lamp with 400 nm cutoff filter), 20 mg catalyst	The degradation efficiency of ~ 91.4% with reaction rate of 0.0064 min^{-1}	[59]
15	TiO_2-MIL-101(Cr)	Gaseous toluene	Two consecutive steps of adsorption and catalysis decomposition Visible light (300 W Xe lamp with 400 nm cutoff filter), 52 MW cm^{-2}, 1000 ppm gaseous toluene, 20 mg catalyst, 480 min irradiation	The degradation efficiency of ~ 90%	[60]

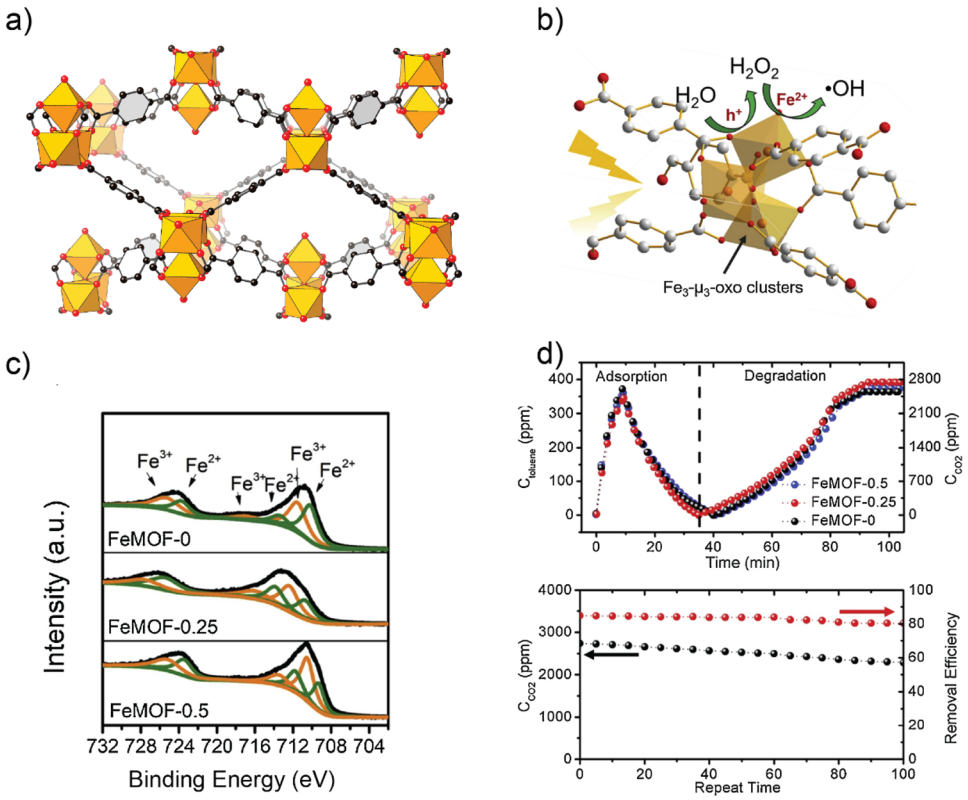

Fig. 1 The crystal structure of MIL-88 (**a**); its Fe2p XPS spectra and the photoactive mechanism (**b**, **c**); and the adsorption and photocatalytic decomposition of toluene (**d**); [Reprinted with permission from Ref. [47]. Copyright 2024, Elsevier]

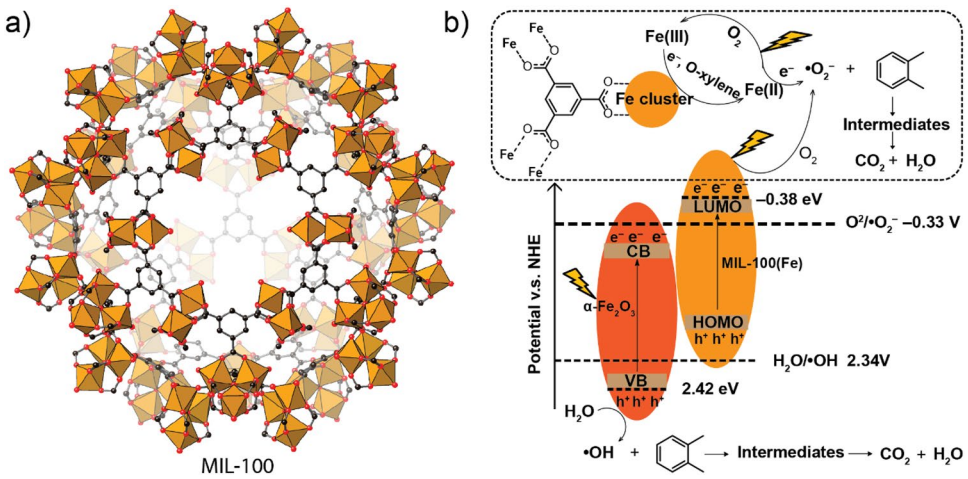

Fig. 2 The structure of MIL-100 (**a**) and its composite with α-Fe_2O_3 (MIL-100(Fe)/α-Fe_2O_3) for photocatalysis oxidation and mineralization of xylene to CO_2 and water (**b**) [49]

Catalysis System Based on Ti-MOFs

Ti-based MOFs were also presented as a highly active class of MOF-based photocatalysts for VOC decomposition. MIL-125(Ti) whose structure is built from Ti-oxo ring cluster and terephthalic acid (H_2BDC) to form 3D architecture with pore sizes of 4.5 Å and 10 Å and pore window of 4 Å is the most common catalyst for aromatic-based VOCs decomposition. This structural motif may have strong interaction with aromatic-based VOCs and the strong active catalytic center based on Ti-cluster. However, they suffers from a slow diffusion rate due to their narrow pore window. To address this limitation, MIL-125 can be modified by introducing defects in the structure (linkers and/or metal clusters), leading to faster diffusion and higher uptake within a limited time, thus enhancing catalytic performance. Jin et al. recently employed a mixed linker strategy using H_2BDC and NH_2-BDC to modify the structure of MIL-125 and generate defect sites for the photocatalytic decomposition of toluene (Fig. 3) [50]. By adjusting the ratio of H_2BDC to 2-aminoterephthalic acid (NH_2-BDC), a tunable hierarchical porosity of MIL-125 can be obtained. Accordingly, the modified

MIL-125 showed toluene mineralization to CO_2 and water with a selectivity of 78%, which was 2.14- and 1.89-fold higher than that of pristine MIL-125 (33.05%) and MIL-125(NH_2) (37.49%), respectively (Table 1, Entry 5) [50].

Utilizing linkers containing a small amount of impurities may also result in the emergence of structural defects, leading to enhanced catalytic performance of MIL-125. Zhang et al. synthesized P-MIL-125 using an H_2BDC linker obtained from plastic hydrolysis (Fig. 4, Table 1, Entry 6) [51]. The impurities present in the linker promoted the formation of structural defects indicated by the emergence of larger pore sizes in P-MIL-125. Moreover, the promoting Lewis acidity of P-MIL-125 was also found, possibly due to the partially replacement of linkers by coordinated impurities at the Ti-metal clusters (such as remaining H_2SO_4 from the acidified step), followed by their release (SO_4^{2-}), which generates structural defects along with the emergence of Lewis sites. This resulted in both stronger interaction via the enhancing Lewis acidity and faster diffusion of aromatic-based VOCs in MOFs. Meanwhile, further optimization of the band gap of P-MIL-125 was carried out through NH_2–H_2BDC linker exchange. This process led to a reduction in the band gap, facilitating easier hydrogen absorption and higher electron transfer efficiency. The system after optimization showed significant enhancement in catalytic performance for the decomposition of toluene and chlorobenzene under visible-light irradiation. Particularly, moderate conversions of 56 and 62% were, respectively, achieved for toluene and chlorobenzene with a reasonable ratio of catalyst/substrates (10 mg catalyst, 1 ml Toluene) together with a short irradiation time (60 min). This result indicated a significant increase in catalytic performance compared to previous studies using MIL-125, which employed a higher catalyst/substrates ratio (200 mg catalyst, 1.0 µL toluene) and longer irradiation (390 min) [51].

Mixing 2D materials with MOFs also enhances the catalytic properties of the resulting composites. Following the success of employing the Ti-based metal–organic framework with a site defects for the photocatalytic decomposition of toluene [50], Park et al. employed MIL-125(H) to synthesize a composite with graphene oxide (Fig. 5) [52]. The presence of graphene oxide (GO) in the system was claimed to enhance charge separation and light adsorption ability, as well as superior photothermal effect of GO. The obtained materials were used as both the adsorbent and the photocatalyst for toluene removal. In their studies, GO nanosheets were integrated with a hierarchical Ti-based MOF (MIL-125 (H)). Under similar conditions, nanosheets integrated with MIL-125 were prepared [50]. The investigation using MIL-125 (H) with 10 wt% GO exhibited enhanced adsorption and photocatalytic mineralization of toluene (79.22%) compared to the pure MIL-125 (when neither pure H_2BDC nor NH_2–BDC linkers were used) and its composite with GO (Table 1, Entry 7) [52]. Despite the initial success, the preparation method suffers from a critical drawback in creating a strong interaction between GO and MIL-125, thus limiting

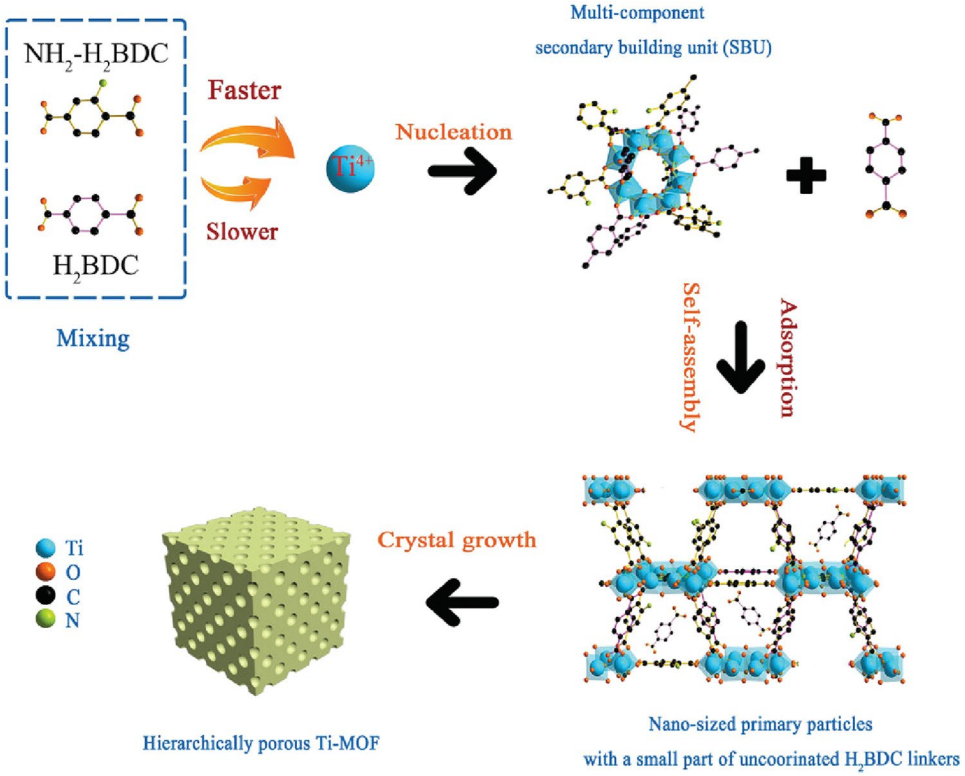

Fig. 3 Mechanism for the formation of structural defects and the origination of hierarchically porous structure of MIL-125 [Reprinted with permission from Ref. [50]. Copyright 2016, John Wiley & Sons]

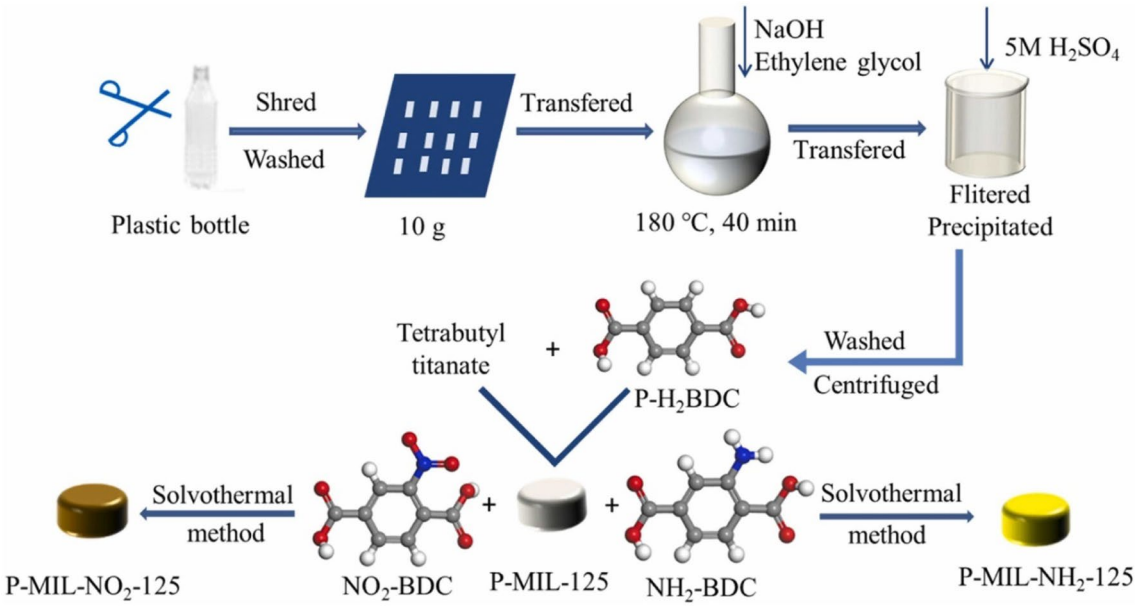

Fig. 4 Synthesis route of P-MIL-NH_2-125 and P-MIL-NO_2-125 from the wasted plastic bottle [Reprinted with permission from Ref. [51]. Copyright 2024, Elsevier]

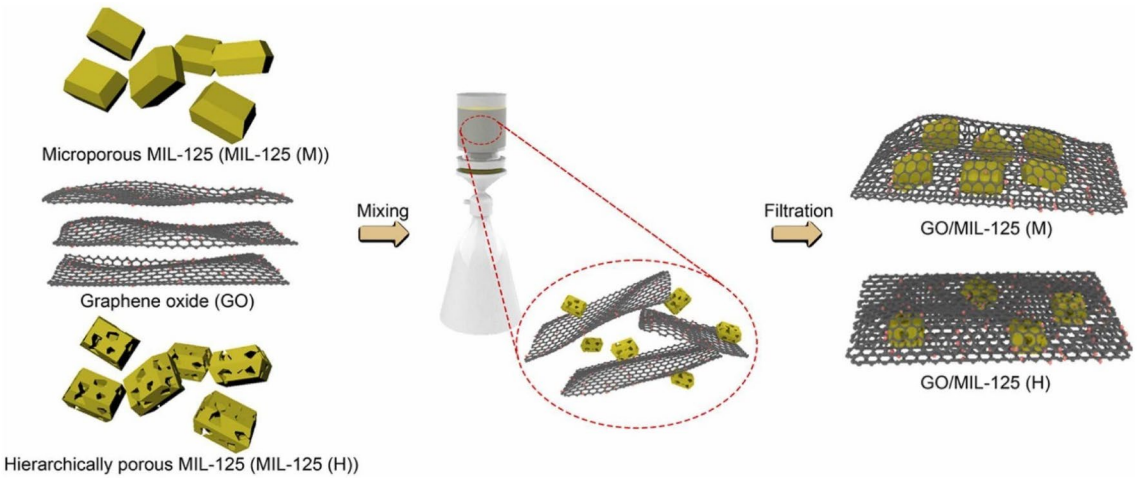

Fig. 5 Preparation process of GO/MIL-125 (M) and GO/MIL-125 (H) hybrids [Reprinted with permission from Ref. [52]. Copyright 2024, Elsevier]

the transportation of electrons between the two components. Developing methods for the direct growth of Ti-MOFs on GO may further enhance the catalytic activity.

Despite significant advancements that have been made, further design of Ti-based MOFs and their composites to boost the catalytic activity for aromatic-based VOC decomposition is highly demanded. Based on the recent advancement, several approaches for structural design and synthesis of Ti-based MOFs with enhancing catalytic performance are highlighted: (i) engineering the structure of Ti-based MOFs to achieve hierarchical structures through mixed linker strategies, reticular design, and/or using organic linkers with a certain level of impurities; (ii) enhancing the Lewis acidity of Ti-cluster by either strong acid coordination (such as H_2SO_4), similar to that of sulfate functionalized in MOF-808, or employing linkers with strong electron withdrawal functionalities; iii) optimizing the band gap using linkers with antenna groups and/or doping exotic components, such as organic/organometallic photo-antenna, nanoparticles, and/or 2D materials via in-situ crystal growing/wrapping to trigger heterojunction mechanism.

Catalysis System Based on Zr-MOFs

Zr-based MOFs are known to be remarkably stable in water under neutral and acidic conditions. Moreover, the adjustable pore size, shape, and chemical properties of the inner surface make this class of MOFs highly suitable for the adsorption of aromatic-based VOCs. Examples of Zr-based MOFs, such as BUT-66, BUT-55 (BUT = Beijing University of Technology), UiO-66 (UiO = Universitetet i Oslo), and MFM-300, are known for their strong affinity toward aromatic-based VOCs [61–63].

Recently, UiO-66 was found to catalyze the toluene decomposition under visible light with the removal efficiency of 69.6% (Table 1, Entry 8). The analysis of samples before and after adsorption showed that the interaction between UiO-66 (Zr) and adsorbed toluene facilitated the charge transfer and prolonged the carrier lifetime, leading to the increase of hydroxyl radicals (·OH) in photocatalysis [53]. Despite these desirable characteristics, Zr-based MOFs exhibit relatively weak photocatalytic activity. Therefore, modification of their properties by doping exotic components is necessary to enhance their application in the photocatalytic decomposition of aromatic-based VOCs.

Nanoparticles incorporated into MOFs are the common and effective photocatalyst system for the decomposition of aromatic-based VOCs. Wrapping MOFs around the catalytic active centers results in the following synergistic effects: (i) MOFs adsorb VOCs in their pores, providing a higher substrate concentration around catalytic active centers; (ii) triggering a heterojunction mechanism involves the cross-transfer of electrons and holes between MOFs and nanoparticles through contact interfaces. TiO_2 nanoparticles (NPs) are a popular choice due to their excellent photocatalytic activity. Zhang et al. investigated the photocatalytic performance of a series of TiO_2@UiO-66 composites under flowing conditions and UV illumination for toluene mineralization [56]. The TiO_2@UiO-66 composites showed a superior and stable photocatalytic activity for toluene conversion. The CO_2 production was 3.27 and 4.10 times higher than that of UiO-66, respectively. The in-situ FT-IR results showed that toluene was oxidized by $O_2^{\cdot-}$ and h^+ to benzaldehyde and benzoic acid, then further oxidized to oxalic acid, and finally mineralized into CO_2 and H_2O (Table 1, Entry 11) [56].

In the same manner, utilization of amine-functionalized linkers resulted in a slight enhancement of catalysis performance due to the better light adsorption behavior of amine groups. Later, Zhang et al. prepared TiO_2–UiO-66–NH_2 nanocomposites for the photocatalytic oxidation of toluene under UV light irradiation with the continuous flow of gaseous toluene (Table 1, Entry 10) [55]. The experimental results revealed that TiO_2–UiO-66–NH_2 exhibited a higher efficiency for toluene removal than TiO_2, UiO-66–NH_2, and other TiO_2-based porous materials for the catalysis period of > 720 min under flowing conditions. Among various materials, the samples containing 75 wt% of UiO-66–NH_2 exhibited the highest photocatalytic activity and CO_2 selectivity with a 72.7% toluene conversion. Its efficiency was 9.7 times higher than that of UiO-66–NH_2. Studying the mechanism through scavenger experiments revealed the involvement of both the $O_2^{\cdot-}$ and h^+ active species in the toluene oxidation. Both UiO-66–NH_2 and TiO_2 were excited under UV irradiation to generate the electron–hole pairs. Subsequently, the electrons at the CB of UiO-66–NH_2 transferred to that of TiO_2 and reacted with O_2 to form $O_2^{\cdot-}$. The h^+ generated at the VB of TiO_2 was transferred to that of UiO-66–NH_2 and directly participated in toluene oxidation (Table 1, Entry 10) [55]. In a similar manner, Yao et al. doped TiO_2 nanoparticles into NH_2-UiO-66 by pre-adsorbing Zr^{4+} to a TiO_2 seed, followed by the solvothermal reaction with linkers to prepare TiO_2@NH_2-UiO-66 [54]. The composite showed a reasonable catalysis activity for styrene photo-decomposition under a visible-light source, despite NH_2-UiO-66 being photo-inactive and TiO_2 only showing good activity under UV light. The TiO_2@NH_2–UiO-66 composites with 5 wt% TiO_2 exhibited a remarkable improvement of the photocatalytic efficiency for styrene mineralization over TiO_2 and NH_2–UiO-66 with the removal ratio of > 99% (to CO_2) for more than 600 min (Table 1, Entry 9) [54].

UiO-66 metal–organic framework gel (MOG) was also employed as a host for doping carbon quantum dots (CQDs), followed by their application in the mineralization of toluene, o-xylene, and styrene (Fig. 6) [57]. The utilization of metal–organic framework gels and xerogels (after solvent removal) offers several major advantages compared with traditional UiO-66 powder owing to the presence of permanent mesopores between particles when their size is below 40 nm, therefore enhancing the mass diffusion of aromatic-based VOCs. Moreover, the nature of xerogel making from exceptional small particles results in the uniform contact of MOFs with exotic components, thus allowing more efficient transfer of electrons and holes between these components to enhance the catalysis activity. Under optimized conditions, the sample containing 0.5 wt% CQDs in UiO-66 MOG exhibited a toluene uptake of 29.06 μmol/g and 4.4 times of degradation enhancement compared to the pristine UiO-66 MOG (Fig. 6, Table 1, Entry 12) [57].

In a different approach, the combination of MOFs with 2D materials through the strong connection between MOF NPs and 2D layers is crucial for enhancing catalysis performance. In this system, the high surface area and active metal clusters of MOFs are exploited for aromatic-based VOC adsorption. Meanwhile, 2D materials play a role in improving the utilization of photogenerated electrons, which will then be transferred to MOFs via the contact surface of two components. Zhang et al. used black phosphorus (BP)

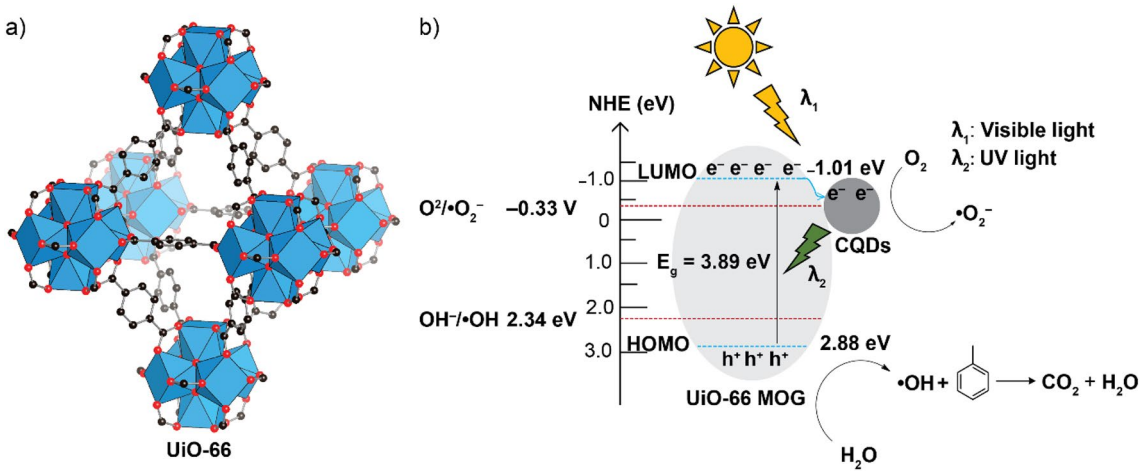

Fig. 6 UiO-66 structure (**a**) and its gel-based composite with CQDs (CQDs/UiO-66 MOG) for the photocatalysis oxidation and mineralization of toluene to CO_2 and water (**b**) [57]

as 2D supporting layers for growing UiO-66 on their surface (Fig. 7) [58]. The Zr atoms formed coordination bonds with the phosphorous atoms. These coordination sites served as the anchoring sites for the growth of the UiO-66 crystals on the BP sheets. The composite was used for the photocatalytic oxidation of toluene and o-dichlorobenzene under visible light. The degradation efficiency of toluene over BP−UiO reached 89.7% with a photocatalytic rate of 0.2840 h^{-1} for toluene, which was 2.17 and 1.34 times faster than that of UiO-66 (0.1311 h^{-1}) and the BP/UiO sample from the traditional blending (0.2076 h^{-1}), respectively. In a similar tendency, the photo-degradation efficiency and rate of o-dichlorobenzene over BP−UiO were up to 91.5% and 1.0419 h^{-1}, respectively, which were 1.68 and 1.35 times faster than UiO-66 (0.6328 h^{-1}) and BP/UiO (0.7745 h^{-1}). The generated CO_2 concentration by BP−UiO, which was higher than that of UiO-66, indicated the faster speed of BP−UiO mineralization. The improved performance of BP−UiO was due to the excellent conductivity of BP, which contributed to improving the utilization of the photogenerated electrons in the system, together with the formation of the coordination bond of the Zr and BP sheets serving as the atomic-level charge-transfer channels from BP to the UiO-66 nanocrystal (Table 1, Entry 13) [58].

In short, the future development of Zr-based MOFs for aromatic-based VOCs decomposition may focus on several key aspects: (i) designing and utilizing Zr-based MOFs, such as BUT-66, which have suitable pore sizes to enhance interaction with aromatic-based VOCs; (ii) synthesizing hierarchical MOFs by controlling defects and/or employing reticular structural designs to enhance diffusion; (iii) tuning the Lewis acidity of Zr-based MOFs to enhance interaction with aromatic-based VOCs through Zr-cluster functionalization with strong acidic moieties and/or using linkers bearing electron withdrawal groups; (iv) engineering the band gap of Zr-based MOFs by incorporating linkers with photo-sensitized groups such as amine functionalities, pyrene, and porphyrin, and/or doping Zr-MOFs by exotic components; (v) synthesizing Zr-MOFs in gel-based forms and their xerogel monoliths to exploit mesopores between particles for enhancing the adsorption/diffusion of aromatic-based VOSs, as well as facilitating their combination with other active components through physical adsorption in mesopores or post-synthetic modifications to anchor active guests via coordination/covalence bonds.

Catalysis System Based on the Other MOFs, and MOF-Based Composites

Aside from the common MOF-based materials from Fe, Ti, and Zr-based MOFs which showed high catalytic activities for aromatic-based VOC decomposition, MOFs synthesized from other metals have received less research attention. The limited focus on exploring catalysis systems based on other metals, such as Co, V, Mn, etc., may hamper attempts to overcome the limitation of the current catalysis system. Indeed, we only found two noticeable examples in the literature, in which the composites of TiO_2 NPs and MIL-101(Cr) were used for toluene oxidation under visible-light irradiation with a degradation efficiency of ~ 90% (Table 1, Entry 14 & 15) [59, 60]. In this system, the authors revealed the dual heterojunction nature of the photocatalysis process, which involved both rutile and anatase phases of TiO_2.

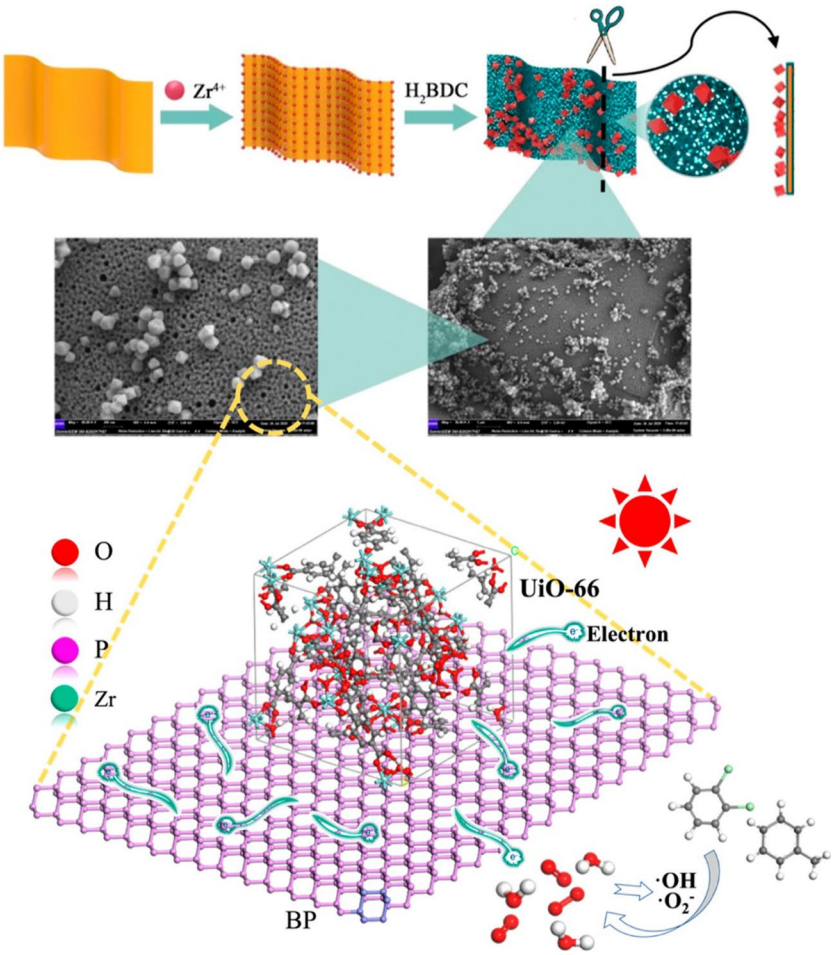

Fig. 7 Schematic illustration for preparation and morphology of UiO-66 on black phosphorus [Reprinted with permission from Ref. [58]. Copyright 2024, American Chemical Society]

MOFs for Thermal Decomposition of Aromatic-Based VOCs

The thermal decomposition of VOCs catalyzed by MOFs has recently garnered interest, particularly concerning VOC mineralization to CO_2 and water. This method involves the VOC decomposition over catalysts at high temperatures, allowing for direct feed of the effluent stream at high temperature to the catalyst converters, thereby saving energy consumption for cooling. Considering the nature of high-temperature operations, this method is an ideal option for treating the exhaust stream of mobile engine or the effluent stream of industrial furnaces/combustions. Among different MOFs, UiO-66 is the most common MOF utilized for this application owing to its remarkable chemical and mechanical stability against oxidation and structural collapse at high temperatures. Cui et al. studied the direct mineralization of toluene under dynamic flow catalyzed by UiO-66 doped with Ag-NPs [64]. In their study, UiO-66 and its encapsulated Ag-nanoparticle analogs were investigated for catalytic activity at high-temperature conditions. The results showed the poor activity of pure UiO-66 with 10% toluene conversion at 400 °C. In contrast, the UiO-66 sample with 10 wt% Ag showed good catalytic performance with a 90% toluene conversion at 295 °C due to the higher lattice oxygen caused by the doped Ag-nanoparticles. However, this catalysis system suffered from the drawbacks of high-temperature working conditions, resulting in the decomposition of the Ag@UiO-66 catalyst (Table 2, Entry 1) [64].

To reduce the working temperature, Bi et al. doped Pd NPs in UiO-66 for direct toluene mineralization under the dynamic flow [65]. A series of Pd nanoparticle-supported UiO-66 catalysts were successfully synthesized by various methods to compare their catalytic activities. Among these catalysts, the Pd–U–EG prepared by reducing Pd^{2+} using ethylene glycol and the Pd–U–NH prepared by reducing Pd^{2+} using $NaBH_4$ exhibited better performances compared to the Pd–U–H prepared by reducing Pd^{2+} under the H_2 gas flow. The results showed the high activities of Pd–U–EG and Pd–U–NH with 90% toluene conversion at 198 and 204 °C, respectively, under 30,000 ml/g/h weight hourly space velocity and 1000 ppm toluene concentration. The improvement of the catalytic activity was attributed to the synergistic effect of the high proportion of Pd^0/Pd^{2+} and

Table 2 MOFs for catalytic thermal decomposition of aromatic-based VOCs

Entry	MOF-based catalysts	VOCs	Catalysis condition	Result	References
1	Ag_{NP}@UiO-66	Toluene	Dynamic adsorption and decomposition at the conc. of 1000 ppm and the flow rate of 50 ml/min Temperature of 295 °C, 0.1 g catalyst	Toluene conversion of 90% Benzaldehyde benzoic acid and CO_2 were detected	[64]
2	Pd_{NP}@UiO-66 (Pd-U-EG)	Toluene	Dynamic adsorption and decomposition at WHSV of 30,000 ml/g/h and conc. of 1000 ppm Temperature of 198 °C, 0.1 g catalyst	Conversion of 90% No decline of the catalysis activity for up to 20 vol.% of water in the feed stream Benzaldehyde, benzoic acid, maleic acid and CO_2 were detected	[65]
3	Pd atoms, clusters, NPs@UiO-66	Toluene	Dynamic adsorption and decomposition at WHSV of 40,000 ml/g/h and conc. of 1000 ppm Temperature of 240 °C, 0.075 g catalyst	Conversion of 90%	[66]
4	Pd atoms, clusters, NPs/UiO-66	Toluene	Fixed bed microreactor (external diameter: 6 mm; inner diameter: 4 mm). Dynamic adsorption and decomposition at WHSV of 30,000 ml/g/h and conc. of 1000 ppm Temperature of 240 °C, 100 mg catalyst	Conversion of ~ 100%	[67]
5	Pt/UiO-66	Toluene	Fixed bed microreactor (U-shaped quartz reaction tube, external diameter: 6 mm; inner diameter: 4 mm). 100 mg catalyst (20–40 mesh) dynamic adsorption and decomposition at WHSV of 40,000 ml/g/h and conc. of 1000 ppm Temperature of 225 °C, 0.1 g catalyst	Conversion of ~ 100% with TOF = 30×10^{-6} s^{-1}	[68]
6	Pd_{NP}@MIL-101(Cr)	Toluene	Two consecutive steps of adsorption and thermal decomposition Temperature > 187 °C	TOF ~ 1.32 $mmol_{toluen}$ mol_{AS}^{-1} s^{-1} Conversion of 80% with selectivity of 73% to CO_2	[69]

the high dispersion of the O_{lat} species. More importantly, Pd–U–EG showed good water resistance, maintaining its catalytic activity without noticeable decline even with up to 20 vol% water in the feed stream. The catalytic stability was also investigated. The results indicated that Pd–U–H and Pd–U–NH exhibited higher stabilities compared to Pd–U–EG. Despite this initial success, new catalysis systems involving the utilization of MOFs must be synthesized to further reduce the operating temperature (Table 2, Entry 2) [65].

Doping Pd into UiO-66 in a controlled manner at low concentration leads to the formation of three different active species: namely, isolated atoms, sub-nanometer clusters, and Pd nanoparticles in the UiO-66 matrix (Table 2, Entry 3) [66]. After consecutive H_2–O_2 and reaction gas activation (1000 ppm toluene in 20 vol% O_2/Ar), this catalyst showed significantly enhanced performance over the original samples for the decomposition of aromatic-based VOCs. Upon completed activation, the sample Pd–U–H–O exhibited high water resistance and superb activity for toluene oxidation, achieving approximately 100% conversion at 240 °C. The enhanced catalytic performance was attributed to the transformation of single Pd atoms into N-complex species, as well as the improved adsorption of toluene owing to the presence of Pd sub-nanometer clusters and nanoparticles [66]. In a subsequent study, the same research group synthesized Pd-doped UiO-66 and its NH_2 and NO_2 analogues, and also conducted a catalysis investigation in the presence of H_2O and SO_2. The results indicated that the Pd-doped UiO-66 catalyst exhibited the highest performance for toluene degradation when compared to its functionalized analogs, maintaining stability in the presence of both water and SO_2 (Table 2, Entry 4) [67]. In the same manner, doping Pt in UiO-66 also enhanced the catalytic performance for toluene degradation, achieving approximately 100% conversion at around 225 °C. Mechanism study revealed a synergistic effect that involved the transformation of Pt^0–PtO, resulting in the formation of oxygen vacancies (Table 2, Entry 5) [68].

In the different studies, Rezaei et al. employed MIL-101 as a host matrix for doping TiO_2 and Pd nanoparticles

[69]. However, the approach in this study utilized a two-step process that involved adsorption and thermal decomposition. The result showed that Pd@MIL-101(Cr) with 0.7 wt% Pd exhibited the best performance by displaying a TOF value of 1.32 $mmol_{toluene}/mol_{AS}/s$, which was 15% and 10% higher than those of pristine MIL-101(Cr) and TiO_2/MIL-101(Cr) with 18 wt% TiO_2. Under optimized conditions at temperature > 187 °C, the toluene conversion was found 80% with 73% selective conversion to CO_2 and H_2O. However, the method suffered from several problems, including the operation condition employed with two separate steps preventing the continuing decomposition of toluene and the thermal desorption and escape of toluene during decomposition at high temperatures (Table 2, Entry 6) [69].

The limited uptake by MOFs during high-temperature operations suggests that their primary function within the system might be to act as a host matrix to prevent active catalytic components from aggregation and/or reacting with each other causing the activity decrease. The future development of MOFs for the thermal decomposition of aromatic-based VOCs, therefore, may focus on several aspects: (i) designing materials that are structurally stable at high temperature together with a slit pore architecture connected by small windows to prevent the aggregation of active components; (ii) enhancing catalytic performance by carefully choosing and distributing the active catalytic components within the MOF structure. The activity of these composite materials largely depends on factors like which catalytic components are used and how they are arranged. For instance, palladium (Pd) in the form of single atoms has been shown to be highly effective for the decomposition of toluene, a common VOC. On the other hand, larger forms of palladium, such as clusters or nanoparticles, may be better at improving the material's ability to adsorb substances at high temperatures. Therefore, improving the catalytic system could involve precise control over these "doped" components—meaning the intentional addition of specific atoms or molecules to enhance certain properties of the MOFs. This can be achieved by the flexibility in controlling the surface properties of MOFs. For example, MOFs can provide active Brønsted acid centers through the coordination of H_2O molecules at the metal clusters, which may serve as anchoring sites for the immobilization of single metal atoms. On the other hand, the presence of basic functionalities such as NH_2 in MOFs may lead to an increase in local pH, causing the deprotonation of coordinated water around the active metal components, followed by the formation of metal oxide nanoparticles. While the quantity and spatial distribution of Brønsted acid centers are determined by the structural architecture, the presence of basic groups can be controlled through mixed linkers' strategies. Thus, this provides a unique approach to controlling the distribution and type of active components in the MOFs matrix to alter catalytic performance.

MOFs for Aromatic-Based VOCs Decomposition Under Non-thermal Plasma Condition

In the non-thermal plasma (NTP) process, the application of high electrical voltage leads to the collision of highly energetic electrons with air molecules, resulting in the formation of reactive species, ions, and radicals. These species participate in the decomposition of oxidized VOCs. However, this method suffers from problems associated with high energy consumption, often low VOC concentrations in ambient air, incomplete oxidation, and the formation of harmful byproducts (e.g., O_3, CO, and NO_x). Consequently, there is a high demand for employing solid adsorbents/catalysts that not only play a role in concentrating VOCs, but also provide catalytically active centers in their structures to achieve complete mineralization of VOCs under NPT conditions.

Haghighat et al. recently utilized a series of MOFs (MIL-101, MIL-53, and CPM-5) as both adsorbents and catalysts in a two-step process: (1) preconcentration of the aromatic-based VOCs via adsorption; and (2) catalytic destruction under NTP conditions [70]. The results of the NTP-catalytic oxidation reactions demonstrated high removal efficiencies of isobutanol (100%) and toluene (~90%) for all three MOFs under dry-air conditions. However, the presence of water moisture at 30% RH led to significant decreases in removal performance. This issue was attributed to the preferable adsorption of H_2O molecules, limiting access of VOC molecules to the active metal centers and/or reducing the effectiveness of high electrical voltage in generating reactive species under humid air. Therefore, further design of MOF adsorbents/catalysts should focus on strengthening interactions with VOCs to enhance uptake capacity at low pressure, improving water-repellent properties of the inner surface, and/or enhancing the activity of catalytic centers [70].

Conclusion

In this review, the recent advances for the decomposition of the aromatic-based VOCs using MOF-based catalysts were summarized. Our viewpoints on the design and synthesis of improved MOF-based photocatalysts include the followings: (i) designing MOFs with suitable micropores decorated by active sites; (ii) promoting mass diffusion through structural defect engineering, reticular structural design, and/or employing xerogel monoliths; (iii) optimizing band gap by selecting appropriate building blocks and/or doping with exotic components. In the subsequent section discussing the

design of MOF-based catalysis for thermal decomposition of aromatic-based VOCs, research efforts should focus on several key factors. First, employing thermally stable MOFs with a slit pore architecture to prevent aggregation of active components. Second, developing methods to control the distribution and type of active components in the MOFs matrix to modify catalytic performance. Our discussion and viewpoints on the design and synthesis of MOFs and MOF-based composites are expected to inspire researchers to design better and more efficient catalysis systems for the decomposition of aromatic-based VOCs.

Acknowledgements This research was supported by the Brainpool Program (NRF 2022H1D3A2A02079453) through the National Research Foundation of Korea (NRF), funded by the Ministry of Science and ICT, and Basic Science Research Capacity Enhancement Project through Korea Basic Science Institute (National research Facilities and Equipment Center) grant funded by the Ministry of Education (2019R1A6C1010052).

Data availability Data generated in this study are available from the corresponding author upon request.

References

1. K. Vellingiri, J.E. Szulejko, P. Kumar, E.E. Kwon, K.H. Kim, A. Deep, D.W. Boukhvalov, R.J.C. Brown, Metal organic frameworks as sorption media for volatile and semi-volatile organic compounds at ambient conditions. Sci. Rep. **6**, 27813 (2016)
2. C.M. Mchale, L. Zhang, M.T. Smith, Current understanding of the mechanism of benzene-induced leukemia in humans: implications for risk assessment. Carcinogenesis **33**, 240 (2012)
3. Y. Miyagi, F. Shima, K. Ishido, T. Yasutake, K. Kamikaseda, Tremor induced by toluene misuse successfully treated by a Vim thalamotomy. J. Neurol. Neurosurg. Psychiatry **66**, 794 (1999)
4. T.H.J. Draper, D.E. Bamiou, Auditory neuropathy in a patient exposed to xylene: case report. J. Laryngol. Otol. **123**, 462 (2009)
5. T.N. Tu, M.V. Nguyen, H.L. Nguyen, B. Yuliarto, K.E. Cordova, S. Demir, Designing bipyridine-functionalized zirconium metal–organic frameworks as a platform for clean energy and other emerging applications. Coord. Chem. Rev. **364**, 33 (2018)
6. H. Furukawa, K.E. Cordova, M. O'Keeffe, O.M. Yaghi, The chemistry and applications of metal-organic frameworks. Science **341**, 1230444 (2013)
7. M. O'Keeffe, M.A. Peskov, S.J. Ramsden, O.M. Yaghi, The reticular chemistry structure resource (RCSR) database of, and symbols for, crystal nets. Acc. Chem. Res. **41**, 1782 (2008)
8. T.A. To, Y.H. Vo, H.T.T. Nguyen, P.T.M. Ha, S.H. Doan, T.L.H. Doan, S. Li, H.V. Le, T.N. Tu, N.T.S. Phan, Iron-catalyzed one-pot sequential transformations: synthesis of quinazolinones via oxidative Csp^3–H bond activation using a new metal-organic framework as catalyst. J. Catal. **370**, 11 (2019)
9. P.H. Pham, S.H. Doan, H.T.T. Tran, N.N. Nguyen, A.N.Q. Phan, H.V. Le, T.N. Tu, N.T.S. Phan, A new transformation of coumarins: via direct C–H bond activation utilizing an iron-organic framework as a recyclable catalyst. Catal. Sci. Technol. **8**, 1267 (2018)
10. H.T.T. Nguyen, T.N. Tu, M.V. Nguyen, T.H.N. Lo, H. Furukawa, N.N. Nguyen, M.D. Nguyen, Combining linker design and linker-exchange strategies for the synthesis of a stable large-pore Zr-based metal-organic framework. ACS Appl. Mater. Interfaces **10**, 35462 (2018)
11. S.H. Doan, N.K.Q. Tran, P.H. Pham, V.H.H. Nguyen, N.N. Nguyen, P.T.M. Ha, S. Li, H.V. Le, N.T.H. Le, T.N. Tu, N.T.S. Phan, A new synthetic pathway to triphenylpyridines via cascade reactions utilizing a new iron-organic framework as a recyclable heterogeneous catalyst. Eur. J. Org. Chem. **2019**, 2382 (2019)
12. T.N. Tu, H.T.T. Nguyen, H.T.D. Nguyen, M.V. Nguyen, T.D. Nguyen, N.T. Tran, K.T. Lim, A new iron-based metal-organic framework with enhancing catalysis activity for benzene hydroxylation. RSC Adv. **9**, 16784 (2019)
13. T.K. Vo, M.T. Nguyen, V.C. Nguyen, J. Kim, Microwave-assisted synthesis of $MgFe_2O_4$-decorated UiO-66(Zr)-NH_2 composites for collaborative adsorption and photocatalytic degradation of tetracycline. Korean J. Chem. Eng. **39**, 2532 (2022)
14. Y. Lin, C. Kong, Q. Zhang, L. Chen, Metal-organic frameworks for carbon dioxide capture and methane storage. Adv. Energy Mater. **7**, 1601296 (2017)
15. Y. He, W. Zhou, G. Qian, B. Chen, Methane storage in metal-organic frameworks. Chem. Soc. Rev. **43**, 5657 (2014)
16. T.N. Tu, H.T.D. Nguyen, N.T. Tran, Tailoring the pore size and shape of the one-dimensional channels in iron-based MOFs for enhancing the methane storage capacity. Inorg. Chem. Front. **6**, 2441 (2019)
17. T.N. Tu, L.H. Ngo, T.T. Nguyen, Metal-organic frameworks as adsorbents for onboard fuel storage. Reticul. Chem. Appl. De Gruyter (2023). https://doi.org/10.1515/9781501524721-008
18. V.N. Le, T.N. Tu, J. Kim, Facile synthesis of Cu-based metal–organic framework/chitosan composite granules for toluene adsorption. Sep. Purif. Technol. **306**, 122718 (2023)
19. V.N. Le, V.C. Nguyen, H.T. Nguyen, H.D. Tran, T.N. Tu, W.S. Kim, J. Kim, Facile synthesis of bimetallic MIL-100(Fe, Al) for enhancing CO_2 adsorption performance. Microporous Mesoporous Mater. **360**, 112716 (2023)
20. M. Allahbakhshi, M. Mosaferi, N.M. Mahmoodi, H. Kazemian, H. Aslani, Functionalized three-dimensional iron-based MIL with high adsorption for removing hazardous organics from water. Korean J. Chem. Eng. **40**, 2892 (2023)
21. K. Adil, Y. Belmabkhout, R.S. Pillai, A. Cadiau, P.M. Bhatt, A.H. Assen, G. Maurin, M. Eddaoudi, Gas/vapour separation using ultra-microporous metal–organic frameworks: insights into the structure/separation relationship. Chem. Soc. Rev. **46**, 3402 (2017)
22. M.I. Gonzalez, M.T. Kapelewski, E.D. Bloch, P.J. Milner, D.A. Reed, M.R. Hudson, J.A. Mason, G. Barin, C.M. Brown, J.R. Long, Separation of xylene isomers through multiple metal site interactions in metal-organic frameworks. J. Am. Chem. Soc. **140**, 3412 (2018)
23. Y. Liu, Z. Chen, G. Liu, Y. Belmabkhout, K. Adil, M. Eddaoudi, W. Koros, Conformation-controlled molecular sieving effects for membrane-based propylene/propane separation. Adv. Mater. **31**, 1807513 (2019)
24. Z.R. Herm, B.M. Wiers, J.A. Mason, J.M.V. Baten, M.R. Hudson, P. Zajdel, C.M. Brown, N. Masciocchi, R. Krishna, J.R. Long, Separation of hexane isomers in a metal-organic framework with triangular channels. Science **340**, 960 (2013)
25. V. Pirouzfar, N. Roustaie, C.H. Su, Gas transport characteristics of mixed matrix membrane containing MIL-100 (Fe) metal-organic frameworks and PEBAX precursors. Korean J. Chem. Eng. **40**, 2138 (2023)
26. P. Yang, R. Zhou, Y. Zhang, S. Cao, D. Zhang, H. Ji, L. Duan, X. Meng, Enhanced CO_2/N_2 separation performance in HP-Cu-BTCs by modifying the open-metal sites and porosity using added templates. Korean J. Chem. Eng. **40**, 675 (2023)
27. T.N. Tu, Y. Shin, S.A. Khalate, K. Chang, H.T. Kwon, J. Kim, Meso/macropore emerging from MOF granulation for enhancing

performance in the Xe/Kr separation. Sep. Purif. Technol. **343**, 127128 (2024)
28. X. Meng, H.-N. Wang, S.-Y. Song, H.-J. Zhang, Proton-conducting crystalline porous materials. Chem. Soc. Rev. **46**, 464 (2017)
29. T.H.N. Lo, M.V. Nguyen, T.N. Tu, An anchoring strategy leads to enhanced proton conductivity in a new metal-organic framework. Inorg. Chem. Front. **4**, 1509 (2017)
30. M.V. Nguyen, T.H.N. Lo, L.C. Luu, H.T.T. Nguyen, T.N. Tu, Enhancing proton conductivity in a metal-organic framework at: T > 80 °C by an anchoring strategy. J. Mater. Chem. **6**, 1816 (2018)
31. T.N. Tu, N.Q. Phan, T.T. Vu, H.L. Nguyen, K.E. Cordova, H. Furukawa, High proton conductivity at low relative humidity in an anionic Fe-based metal-organic framework. J. Mater. Chem. A **4**, 3638 (2016)
32. I.A. Lázaro, C.J.R. Wells, R.S. Forgan, Multivariate modulation of the Zr MOF UiO-66 for defect-controlled combination anticancer drug delivery. Angew. Chem. Int. **59**, 5211 (2020)
33. W. Cai, J. Wang, C. Chu, W. Chen, C. Wu, G. Liu, Metal-organic framework-based stimuli-responsive systems for drug delivery. Adv. Sci. **6**, 1801526 (2019)
34. K. Lu, T. Aung, N. Guo, R. Weichselbaum, W. Lin, Nanoscale metal-organic frameworks for therapeutic, imaging, and sensing applications. Adv. Mater. **30**, 1707634 (2018)
35. T.N. Tu, M. Scheer, A novel crystalline template for the structural determination of flexible chain compounds of nanoscale length. Chem **9**, 227 (2023)
36. T.N. Tu, S.A. Khalate, K. Chang, J. Kim, "Ship-in-a-bottle" entrapment of biomolecules in MOF-based xerogel monoliths for high-performance electrochemical hydrogen evolution. J. Mater. Chem. A **12**, 7622 (2024)
37. T.N. Tu, T.M. Pham, Q.H. Nguyen, N.T. Tran, V.N. Le, L.H. Ngo, K. Chang, J. Kim, Metal–organic frameworks for aromatic-based VOC capture. Sep. Purif. Technol. **333**, 125883 (2024)
38. M. Wen, G. Li, H. Liu, J. Chen, T. An, H. Yamashita, Metal-organic framework-based nanomaterials for adsorption and photocatalytic degradation of gaseous pollutants: recent progress and challenges. Environ. Sci. Nano **6**, 1006 (2019)
39. Q. Wang, Q. Gao, A.M. Al-Enizi, A. Nafady, S. Ma, Recent advances in MOF-based photocatalysis: environmental remediation under visible light. Inorg. Chem. Front. **7**, 300 (2020)
40. Y. Jin, H. Liu, M. Feng, Q. Ma, B. Wang, Metal-organic frameworks for air pollution purification and detection. Adv. Funct. Mater. **34**, 2304773 (2023)
41. Q. Du, R. Rao, F. Bi, Y. Yang, W. Zhang, Y. Yang, N. Liu, X. Zhang, Preparation of modified zirconium-based metal-organic frameworks (Zr-MOFs) supported metals and recent application in environment: a review and perspectives. Surf. Interfaces **28**, 101647 (2022)
42. K. Yue, X. Zhang, S. Jiang, J. Chen, Y. Yang, F. Bi, Y. Wang, Recent advances in strategies to modify MIL-125 (Ti) and its environmental applications. J. Mol. Liq. **335**, 116108 (2021)
43. Z. Zhao, S. Ma, B. Gao, F. Bi, R. Qiao, Y. Yang, M. Wu, X. Zhang, A systematic review of intermediates and their characterization methods in VOCs degradation by different catalytic technologies. Sep. Purif. Technol. **314**, 123510 (2023)
44. R. Rao, S. Ma, B. Gao, F. Bi, Y. Chen, Y. Yang, N. Liu, M. Wu, X. Zhang, Recent advances of metal-organic framework-based and derivative materials in the heterogeneous catalytic removal of volatile organic compounds. J. Colloid Interface Sci. **636**, 55 (2023)
45. D. Wang, C. Yuan, C. Yang, P. Wang, Y. Zhan, N. Guo, L. Jiang, Z. Wang, Z. Wang, Recent advances in catalytic removal volatile organic compounds over metal–organic framework–derived catalysts: a review. Sep. Purif. Technol. **326**, 124765 (2023)
46. Z. Zhang, X. Li, B. Liu, Q. Zhao, G. Chen, Hexagonal microspindle of NH_2-MIL-101(Fe) metal-organic frameworks with visible-light-induced photocatalytic activity for the degradation of toluene. RSC Adv. **6**, 4289 (2016)
47. P. Li, S. Kim, J. Jin, H.C. Do, J.H. Park, Efficient photodegradation of volatile organic compounds by iron-based metal-organic frameworks with high adsorption capacity. Appl. Catal. B Environ. **263**, 118284 (2020)
48. J. Lee, J. Jang, J. Kim, S.H. Lim, A recyclable indoor air filter system based on a photocatalytic metal–organic framework for the removal of harmful volatile organic compounds. Chem. Eng. J. **430**, 132891 (2022)
49. L. Chen, X. Wang, Z. Rao, Z. Tang, Y. Wang, G. Shi, G. Lu, X. Xie, D. Chen, J. Sun, In-situ synthesis of Z-Scheme MIL-100(Fe)/α-Fe_2O_3 heterojunction for enhanced adsorption and Visible-light photocatalytic oxidation of O-xylene. Chem. Eng. J. **416**, 129112 (2021)
50. J. Jin, P. Li, D.H. Chun, B. Jin, K. Zhang, J.H. Park, Defect dominated hierarchical ti-metal-organic frameworks via a linker competitive coordination strategy for toluene removal. Adv. Funct. Mater. **31**, 2102511 (2021)
51. X. Zhang, K. Yue, R. Rao, J. Chen, Q. Liu, Y. Yang, F. Bi, Y. Wang, J. Xu, N. Liu, Synthesis of acidic MIL-125 from plastic waste: significant contribution of N orbital for efficient photocatalytic degradation of chlorobenzene and toluene. Appl. Catal. B Environ. **310**, 121300 (2022)
52. J. Jin, J.P. Kim, S. Wan, K.H. Kim, Y. Choi, P. Li, J. Kang, Z. Ma, J.H. Lee, O. Kwon, D.W. Kim, J.H. Park, Hierarchical pore enhanced adsorption and photocatalytic performance of graphene oxide/Ti-based metal-organic framework hybrid for toluene removal. Appl. Catal. B Environ. **317**, 121751 (2022)
53. J. Yu, X. Wang, Y. Wang, X. Xie, H. Xie, N. Vorayos, J. Sun, Heating-induced adsorption promoting the efficient removal of toluene by the metal-organic framework UiO-66 (Zr) under visible light. J. Colloid Interface Sci. **653**, 1478 (2024)
54. P. Yao, H. Liu, D. Wang, J. Chen, G. Li, T. An, Enhanced visible-light photocatalytic activity to volatile organic compounds degradation and deactivation resistance mechanism of titania confined inside a metal-organic framework. J. Colloid Interface Sci. **522**, 174 (2018)
55. J. Zhang, Y. Hu, J. Qin, Z. Yang, M. Fu, TiO_2-UiO-66-NH_2 nanocomposites as efficient photocatalysts for the oxidation of VOCs. Chem. Eng. J. **385**, 123814 (2020)
56. J. Zhang, Z. Guo, Z. Yang, J. Wang, J. Xie, M. Fu, Y. Hu, TiO_2@UiO-66 composites with efficient adsorption and photocatalytic oxidation of VOCs: investigation of synergistic effects and reaction mechanism. ChemCatChem **13**, 581 (2021)
57. J. Yu, X. Wang, L. Chen, G. Lu, G. Shi, X. Xie, Y. Wang, J. Sun, Enhanced adsorption and visible-light photocatalytic degradation of toluene by CQDs/UiO-66 MOG with hierarchical pores. Chem. Eng. J. **435**, 135033 (2022)
58. J. Chen, Y. Yang, S. Zhao, F. Bi, L. Song, N. Liu, J. Xu, Y. Wang, X. Zhang, Stable black phosphorus encapsulation in porous mesh-like UiO-66 promoted charge transfer for photocatalytic oxidation of toluene and o-dichlorobenzene: performance, degradation pathway, and mechanism. ACS Catal. **12**, 8069 (2022)
59. X. Zhang, Z. Zhu, R. Rao, J. Chen, X. Han, S. Jiang, Y. Yang, Y. Wang, L. Wang, Highly efficient visible-light-driven photocatalytic degradation of gaseous toluene by rutile-anatase TiO2@MIL-101 composite with two heterojunctions. J. Environ. Sci. **134**, 21 (2023)
60. J. Chen, X. Zhang, X. Shi, F. Bi, Y. Yang, Y. Wang, Synergistic effects of octahedral TiO_2-MIL-101(Cr) with two heterojunctions for enhancing visible-light photocatalytic degradation of liquid tetracycline and gaseous toluene. J. Colloid Interface Sci. **579**, 37 (2020)

61. L.H. Xie, X.M. Liu, T. He, J.R. Li, Metal-organic frameworks for the capture of trace aromatic volatile organic compounds. Chem **4**, 1911 (2018)
62. Y. Han, Y. Chen, Y. Ma, J. Bailey, Z. Wang, D. Lee, A.M. Sheveleva, F. Tuna, E.J.L. McInnes, M.D. Frogley, S.J. Day, S.P. Thompson, B.F. Spencer, M. Nikiel, P. Manuel, D. Crawshaw, M. Schröder, S. Yang, Control of the pore chemistry in metal-organic frameworks for efficient adsorption of benzene and separation of benzene/cyclohexane. Chem **9**, 739 (2023)
63. T. He, X.J. Kong, Z.X. Bian, Y.Z. Zhang, G.R. Si, L.H. Xie, X.Q. Wu, H. Huang, Z. Chang, X.H. Bu, M.J. Zaworotko, Z.R. Nie, J.R. Li, Trace removal of benzene vapour using double-walled metal–dipyrazolate frameworks. Nat. Mater. **21**, 689 (2022)
64. X. Zhang, L. Song, F. Bi, D. Zhang, Y. Wang, L. Cui, Catalytic oxidation of toluene using a facile synthesized Ag nanoparticle supported on UiO-66 derivative. J. Colloid Interface Sci. **571**, 38 (2020)
65. F. Bi, X. Zhang, J. Chen, Y. Yang, Y. Wang, Excellent catalytic activity and water resistance of UiO-66-supported highly dispersed Pd nanoparticles for toluene catalytic oxidation. Appl. Catal. B Environ. **269**, 118767 (2020)
66. X. Zhang, F. Bi, Z. Zhao, Y. Yang, Y. Li, L. Song, N. Liu, J. Xu, L. Cui, Boosting toluene oxidation by the regulation of Pd species on UiO-66: synergistic effect of Pd species. J. Catal. **413**, 59 (2022)
67. F. Bi, Z. Zhao, Y. Yang, Q. Liu, W. Huang, Y. Huang, X. Zhang, Efficient degradation of toluene over ultra-low Pd supported on UiO-66 and its functional materials: reaction mechanism, water-resistance, and influence of SO_2. Environ. Funct. Mater. **1**, 166 (2022). https://doi.org/10.1016/j.efmat.2022.07.002
68. Y. Yang, D. Zhang, W. Ji, F. Bi, L. Song, X. Zhang, Uniform platinum nanoparticles loaded on Universitetet i Oslo-66 (UiO-66): active and stable catalysts for gas toluene combustion. J. Colloid Interface Sci. **606**, 1811 (2022)
69. B.O. Adebayo, A. Krishnamurthy, Q. Al-Naddaf, A.A. Rownaghi, F. Rezaei, Investigation of combined capture-destruction of toluene over Pd/MIL-101 and TiO_2/MIL-101 dual function materials. Energy Fuel **35**, 13256 (2021)
70. M. Bahri, F. Haghighat, S. Rohani, H. Kazemian, Metal organic frameworks for gas-phase VOCs removal in a NTP-catalytic reactor. Chem. Eng. J. **320**, 308 (2017)